Fabrication and characterization of Co40Fe22Ta8-xYxB30 (x=0, 2.5, 4, 6, and 8) metallic glasses with high thermal stability and good soft magnetic properties

Amir Hossein Taghvaei, Hamed Shakur Shahabi, Jozef Bednarčik, and Jürgen Eckert

Citation: Journal of Applied Physics **116**, 184904 (2014); doi: 10.1063/1.4901266
View online: http://dx.doi.org/10.1063/1.4901266
View Table of Contents: http://scitation.aip.org/content/aip/journal/jap/116/18?ver=pdfcov
Published by the AIP Publishing

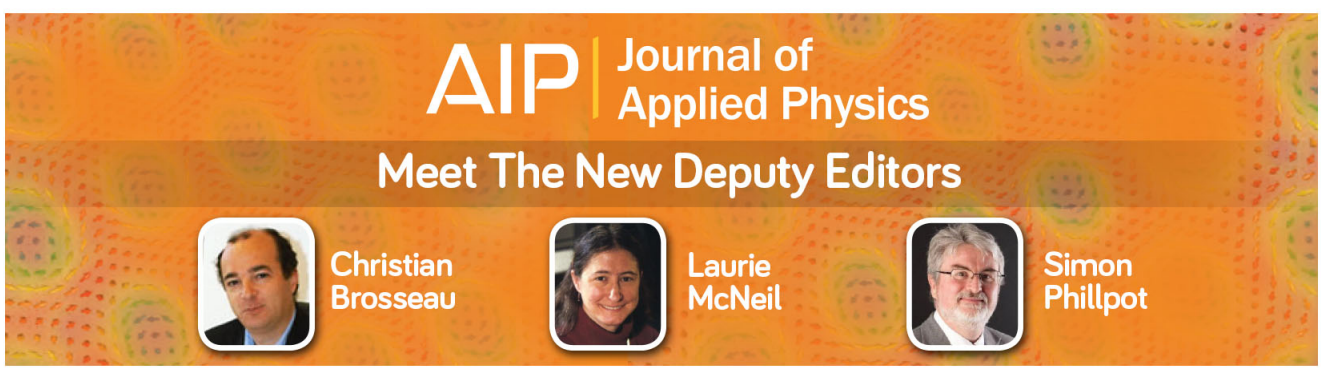

Fabrication and characterization of $Co_{40}Fe_{22}Ta_{8-x}Y_xB_{30}$ (x = 0, 2.5, 4, 6, and 8) metallic glasses with high thermal stability and good soft magnetic properties

Amir Hossein Taghvaei,[1,a)] Hamed Shakur Shahabi,[2] Jozef Bednarčik,[3] and Jürgen Eckert[2,4]
[1]*Department of Materials Science and Engineering, Shiraz University of Technology, Shiraz, Iran*
[2]*IFW Dresden, Institute for Complex Materials, Helmholtzstr. 20, 01069 Dresden, Germany*
[3]*Deutsches Elektronen-Synchrotron DESY, Photon Science, Notkestraße 85, 22603 Hamburg, Germany*
[4]*TU Dresden, Institute of Materials Science, 01062 Dresden, Germany*

(Received 9 September 2014; accepted 28 October 2014; published online 12 November 2014)

Atomic structure and thermal behavior of $Co_{40}Fe_{22}Ta_{8-x}Y_xB_{30}$ (x = 0, 2.5, 4, 6, and 8) metallic glasses with good soft magnetic properties have been investigated by high-energy synchrotron X-ray diffraction and differential scanning calorimeter, respectively. It has been shown that the extension of the supercooled liquid region first increases and reaches a large value of 95 K and subsequently decreases as a function of Y content. Analysis of the structure factors and pair correlation functions in the reciprocal-space and real-space have indicated that the addition of Y noticeably changes the atomic structure and reduces the degree of the medium-range order. Magnetic measurements have implied that the introduction of Y enhances both saturation magnetization and Curie temperatures of the ribbons, while keeping their coercivity very small. The underlying mechanisms for changes in the atomic structure, improving the thermal stability and magnetic properties upon Y addition have been discussed. © *2014 AIP Publishing LLC*.
[http://dx.doi.org/10.1063/1.4901266]

I. INTRODUCTION

Metallic glasses (MGs) exhibit promising physical and mechanical properties compared to their crystalline counterparts.[1,2] They can show a super high strength, large elastic limit, good wear and corrosion resistance, and excellent soft magnetic properties.[1–3] It is known that many properties of such materials strongly depend on their electronic and atomic structural features such as the bonding nature among the constituent elements and the degree of the ordering over the short-range or medium-range scales.[3] One of the important methods to improve the glass forming ability (GFA), thermal stability and properties of MGs is microalloying or changing the chemical composition through a minor addition of some elements.[4] The microalloying can result in formation of the glassy structure with a higher packing density and new local atomic configurations with strong interactions, which can improve the GFA and thermal stability.[4] On the other hand, the microalloying can influence the bonding nature, which affects the local ordering, elastic constants, and in some cases makes the glassy structure heterogeneous which altogether improve the mechanical properties of the MGs.[4–7]

Co-based MGs are well-known alloys owing to their excellent soft magnetic properties, e.g., very small magnetic coercivity, high magnetic permeability, and moderate saturation polarization.[8–10] Such properties make them as an ideal candidate for some applications like magnetic sensors, memories, and power devices.[10,11] It has been demonstrated that the increase of metalloid content especially B up to about 30 at. % can enhance their thermal stability, electrical resistivity, and mechanical properties.[8,12,13] For instance, Inoue *et al.*[14] discovered 2 mm $Co_{43}Fe_{20}Ta_{5.5}B_{31.5}$ glassy rods with very high fracture strength of about 5 GPa and maximum permeability of 550 000. Recently, we have found that the increase of Ta up to 8 at. % results in formation of the $Co_{40}Fe_{22}Ta_8B_{30}$ MGs with a significantly better thermal stability but almost the same magnetic properties as the well-known $Co_{43}Fe_{20}Ta_{5.5}B_{31.5}$ MG.[15] Moreover, the $Co_{40}Fe_{22}Ta_8B_{30}$ bulk glassy alloy with 10 mm diameter indicating ultrahigh hardness, excellent thermal stability, and soft magnetic properties has been fabricated by powder metallurgy method.[16] It would be possible that thermal stability and magnetic properties of the $Co_{40}Fe_{22}Ta_8B_{30}$ MG can be further improved by microalloying through (partial) substitution of Ta with another element. In the current research, Y was selected as substituting atom owing to its larger atomic radii (180 pm (Ref. 17)) compared to other constituent elements and its large negative heat of mixing with B and Co.[18] We expected that the addition of Y can produce new atomic pairs and enhances the sequential variations in the atomic size, which results in a denser topological configuration of atoms in the glassy phase and consequently a better thermal stability. As a result, $Co_{40}Fe_{22}Ta_{8-x}Y_xB_{30}$ (x = 0, 2.5, 4, 6, and 8) glassy ribbons were produced and their atomic structure, thermal stability, and magnetic properties were investigated.

II. EXPERIMENTAL PROCEDURE

The master alloys with nominal compositions $Co_{40}Fe_{22}Ta_{8-x}Y_xB_{30}$ (at. %) (x = 0, 2.5, 4, 6, and 8) were prepared by arc-melting of the pure Co (99.9%), Fe (99.9%), Ta (99.9%),

a)Author to whom correspondence should be addressed. Electronic mail: amirtaghvaei@gmail.com

Y (99%), and crystalline B (99%) under a Ti-gettered argon atmosphere. The obtained ingots were remelted at least three times to improve their homogeneity. Glassy ribbons were obtained under an argon flow by a single-roller Bühler melt-spinner on a copper wheel at 41 m/s tangential wheel velocity.

The phase analysis of the ribbons was carried out by X-ray diffraction (XRD) in reflection geometry, using Co K_α radiation ($\lambda = 0.17889$ nm) and in transmission geometry, using a monochromatic high-energy synchrotron radiation ($\lambda = 0.0123984$ nm) of 100 keV, at the P07 beam line of PETRA III electron storage ring (DESY, Hamburg, Germany). The illumination of the ribbons at room temperature was carried out for 20 s using an incident beam collimated properly with a cross-section of $1 \times 1\,mm^2$. A 2-dimensional (2D) detector (Perkin Elmer 1621) placed orthogonal to the X-ray beam was used to record the XRD patterns. The distance of 60 cm was selected between sample and detector in order to achieve the large wave vectors q ($q = \frac{4\pi \sin\theta}{\lambda}$) up to $180\,nm^{-1}$. The 2D XRD patterns were integrated to the q-space, using FIT2D software package.[19] The elastically scattered intensities were obtained by PDFgetX2 software[20] from the integrated data after performing the different corrections described elsewhere.[16] The total structure factors, $S(q)$, of the as-cast ribbons were calculated from their elastically scattered intensities according to the Faber-Ziman method.[21] The reduced pair correlation functions, $G(r)$, of the as-quenched ribbons were determined from the Fourier transform of $S(q)$ as

$$G(r) = \frac{2}{\pi}\int_{q_{min}}^{q_{max}} q\big(S(q)-1\big)\sin(qr)dq. \quad (1)$$

The thermal behavior of the ribbons was evaluated by a differential scanning calorimeter (DSC, NETZSCH 404) at a constant heating rate of 20 K/min under flow of a purified Ar. The Hysteresis curves and saturation magnetization of the ribbons were measured by a vibrating sample magnetometer (VSM). The coercivity was determined by a Foerster Coercimat under a magnetic field sufficient for saturating the ribbons. The thermomagnetic behavior and Curie temperature of the ribbons were recorded by a Faraday magnetometer at a constant heating rate of 10 K/min. The measurement errors are within ±1.5 K for the DSC and Curie temperature, ±0.1 A/m for coercivity, and ±0.5 Am^2/kg for saturation magnetization.

III. RESULT AND DISCUSSIONS

A. Thermal behavior

The XRD patterns of the as-quenched $Co_{40}Fe_{22}Ta_{8-x}Y_xB_{30}$ ribbons are shown in Fig. 1. Formation of only broad halo pattern without any appreciable Bragg peak for each composition reveals that the prepared ribbons have a fully glassy structure and addition of Y element does not induce any crystallization. Figure 2 shows the DSC plots of the as-cast $Co_{40}Fe_{22}Ta_{8-x}Y_xB_{30}$ ribbons measured at a constant heating rate of 20 K/min. All the compositions except the Ta free alloy (x = 8) indicate a distinct endothermic peak corresponding to

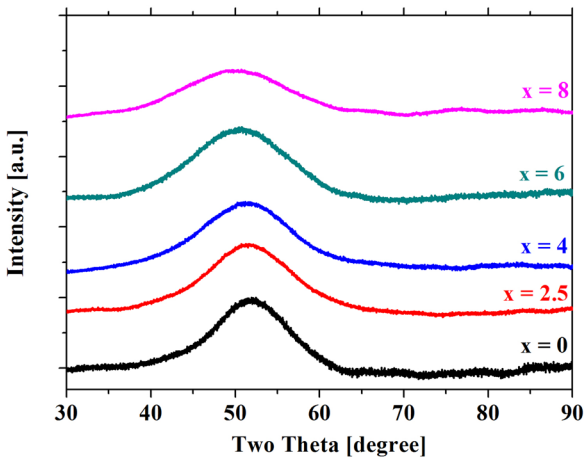

FIG. 1. The XRD patterns of the $Co_{40}Fe_{22}Ta_{8-x}Y_xB_{30}$ (x = 0, 2.5, 4, 6, and 8) glassy ribbons measured in a reflection mode using Co K_α radiation.

the glass transition temperature, T_g, followed by a supercooled liquid region (SLR), ΔT_x ($\Delta T_x = T_{x1} - T_g$, that T_x is the crystallization temperature, measured as the onset of the first exothermic event). According to Fig. 2, the crystallization in Y free alloy (x = 0) proceeds through three stages of exothermic reactions. However, by addition of Y, the second and third exothermic events become weaker and the crystallization takes place through almost a single sharp exothermic peak. The thermal parameters of the as-quenched ribbons are listed in Table I. From this table, it is observed that by addition of Y, the T_g progressively decreases, while the T_{x1} is first enhanced and reaches a maximum value of 984 K for x = 2.5 and subsequently decreases. It is seen that the glassy alloy with x = 2.5 exhibits a largest ΔT_x of 95 K and consequently the highest thermal stability among other compositions investigated in the present work.

In order to identify the phases formed during crystallization, the ribbons were heated isochronally up to the end of primary crystallization peak and subsequently cooled down to room temperature. Figure 3 shows the XRD patterns of the partially devitrified $Co_{40}Fe_{22}Ta_{8-x}Y_xB_{30}$ ribbons. For the Y free alloy, dominant phase is the $(Co,Fe)_{21}Ta_2B_6$ with a face-centered cubic (FCC) structure.[8] In addition, small

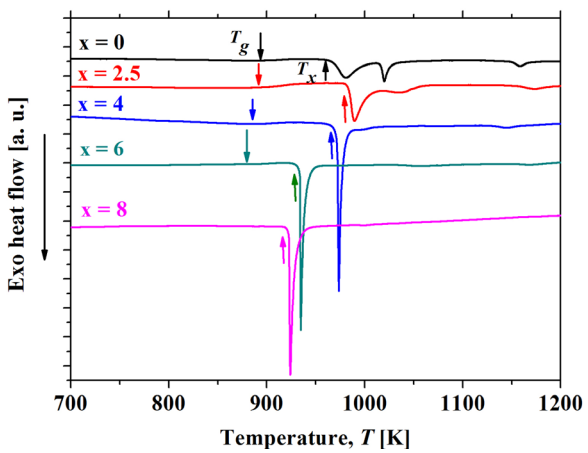

FIG. 2. The DSC plots of the $Co_{40}Fe_{22}Ta_{8-x}Y_xB_{30}$ (x = 0, 2.5, 4, 6, and 8) glassy ribbons measured at a constant heating rate of 20 K/min.

TABLE I. Thermal stability parameters and magnetic properties of the $Co_{40}Fe_{22}Ta_{8-x}Y_xB_{30}$ (x = 0, 2.5, 4, 6, and 8) glassy ribbons. T_g is the glass transition temperature, T_{x1} is the onset of the first crystallization temperature, ΔT_x is the extension of the supercooled liquid region, M_s is the saturation magnetization, T_c is the Curie temperature, and H_c is the coercivity.

Atomic fraction, x	T_g (K)	T_{x1} (K)	$\Delta T_x = T_{x1} - T_g$ (K)	M_s (Am^2/kg)	T_c (K)	H_c (A/m)	References
0	893	967	74	42.4	412	0.8	16
2.5	889	984	95	45.5	420	0.7	Present study
4	885	972	87	53.7	462	0.8	Present study
6	880	934	54	54.3	466	0.9	Present study
8	…	923	…	63.6	488	1.1	Present study

amount of the $(Co,Fe)_3B_2$ phase forms near the end of the first crystallization event.[22] The $(Co,Fe)_{21}Ta_2B_6$ phase has the $Cr_{23}C_6$ prototype structure with the Fm3m space group and a large lattice parameter of 1.055 nm, which contains 116 atoms in each unit cell.[23] By introduction of 2.5 at. % Y, the $(Co,Fe)_{21}(Ta,Y)_2B_6$ phase appears after heating above the first crystallization event. The participation of Y in the complex boride phase can be found from a small shifting in the position of the $(Co,Fe)_{21}Ta_2B_6$ peaks to the lower angles (see Fig. 3) owing to the increased lattice parameter of this phase. In the $Cr_{23}C_6$ prototype structure, it has been shown that the transition or rare-earth elements with large atomic radii such as Ta and Y prefer to occupy the 8*c* sites, while Fe/Co atoms occupy 4*a*, 32*f*, and 48*h* sites.[24,25] Adding more Y (x > 2.5) is responsible for formation of the Co_3YB_2 compound besides the $(Co,Fe)_{21}(Ta,Y)_2B_6$ phase and the fraction of the former phase enhances with increasing Y (see Fig. 3). For the alloy with x = 6, a new phase corresponding to the α-(Fe,Co) solid solution precipitates. For x = 8, the amorphous phase transforms in an eutectic mode to a mixture of Co_3YB_2, (Fe,Co) and tetragonal $(Co,Fe)_2B$ phases after crystallization. According to Fig. 3, it is obvious that the fraction of the complex $(Co,Fe)_{21}(Ta,Y)_2B_6$ phase reduces with

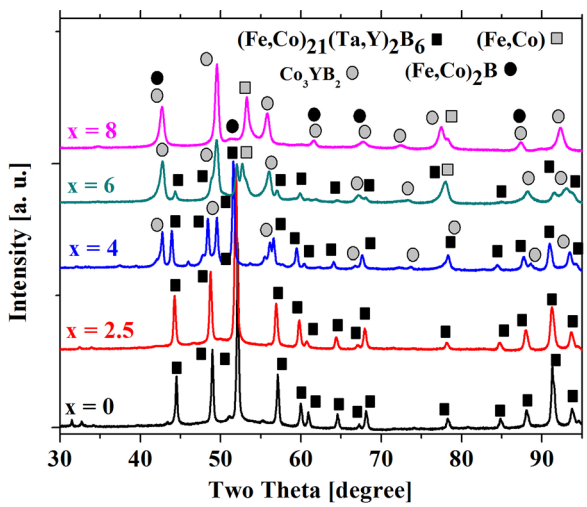

FIG. 3. The XRD patterns (Co K_z radiation) of the partially crystallized $Co_{40}Fe_{22}Ta_{8-x}Y_xB_{30}$ (x = 0, 2.5, 4, 6, and 8) ribbons obtained by isochronal annealing up to the end of their primary crystallization event and subsequently cooled down to room temperature.

increasing Y and the Ta free composition does not show any boride compound with the $Cr_{23}C_6$ structure. It has been suggested that the presence of some elements such as Nb or Ta in Fe-based or Co-based glasses plays a crucial role in formation of borides with the $Cr_{23}C_6$ structure.[8,26]

Formation of the complex FCC $(Co,Fe)_{21}(Ta,Y)_2B_6$ phase upon primary crystallization is correlated with high thermal stability in the present glassy alloys. Due to a complex crystal structure and a large number of atoms in the unit cell of the $(Co,Fe)_{21}(Ta,Y)_2B_6$ phase, its precipitation requires long-range rearrangements of the constituent elements especially when there is a significant difference between the atomic structure of the glassy phase and the precipitating crystals. It is known that the metal-metalloid type glassy alloys usually have a network-like short-range order (SRO), which is fundamentally different with respect to the crystals with $Cr_{23}C_6$ structure.[27,28] Since Y has a largest atomic radii (180 pm) among the constituents in this alloying system, small addition of Y can give rise to a more consecutive change in the atomic size in the order of Y > Ta > Co > Fe > B. Furthermore, Y has a large negative heat of mixing with B (−50 kJ/mol) and Co (−22 kJ/mol) and small mixing enthalpy with Fe (−1 kJ/mol).[18] Hence, a minor addition of Y results in formation of an amorphous phase with a larger thermal stability due to a high packing density and new local atomic configurations with strong interactions, which can dramatically suppress the diffusivity of the elements. Poon *et al*. have suggested that the large (*L*) and small (*S*) atoms can form strong *L*-*S* percolating network or reinforced "backbone" in the amorphous structure.[29] In the current alloying system, due to a large negative heat of mixing between the large Y or Ta and small B atoms, strong Y-B and Ta-B percolating networks can be created. It has been shown that in the $(Co,Fe)_{21}Ta_2B_6$ structure, the Ta atoms located in 8*c* sites have the largest interatomic spacing with B atoms (0.3737 nm), which occupy the 24 *e* site and consequently the Ta-B bond is absent.[23,30] As Y atoms are also located in the 8*c* site, the absence of the Y-B bond is expectable in the $(Co,Fe)_{21}(Ta,Y)_2B_6$ phase. Hence, formation of the $(Co,Fe)_{21}(Ta,Y)_2B_6$ phase upon devitrification needs breaking strong Y-B and Ta-B pairs in the glassy structure before long-range diffusion of Y and Ta atoms with small diffusivity, which contributes to a large thermal stability of the present glassy alloys.

According to Table I, excessive addition of Y (x > 2.5) decreases the thermal stability of the ribbons probably due to decreased fraction of the $(Co,Fe)_{21}(Ta,Y)_2B_6$ phase and formation of less complex phases such as Co_3YB_2, (Co,Fe), and $(Co,Fe)_2B$, which can be precipitated easier. The decrease in T_g upon increasing the Y fraction (see Table I) can be correlated with the changes occurred in the bonding nature and atomic interactions. The mixing enthalpies between Ta and Co, Fe, and B are −24, −15, and −54 kJ/mol, respectively.[18] These values are larger than the mentioned mixing enthalpies between Y and other constituents in the present alloying system. This means that a large Y addition results in formation of an amorphous structure with weaker atomic interactions and consequently there is a lower activation barrier against configuration changes of the glass to occur, causing a decrease in T_g.[31,32]

B. Atomic structure

Figure 4 shows the total structure factors $S(q)$ of the as-quenched $Co_{40}Fe_{22}Ta_{8-x}Y_xB_{30}$ glassy ribbons. It can be seen that all patterns indicate prominent oscillations up to $q \approx 160\,nm^{-1}$. Furthermore, addition of Y affects the shape and position of the diffuse peaks in the entire q range, indicating the changes in atomic structure of the glassy phase. According to Fig. 4, the second diffuse peak of $S(q)$ for the Y free alloy has a strong shoulder around $q = 60\,nm^{-1}$ and the intensity of this shoulder decreases progressively by addition of Y. Moreover, the Ta free alloy exhibits a shoulder on the third peak of the $S(q)$ around $q = 70\,nm^{-1}$, which is not appearing for the Ta bearing alloys. The vanishing of the shoulder of the second $S(q)$ peak was observed by partial replacement of Fe with lanthanide elements such as Sm, Tb, and Dy in the $Fe_{70}Co_{10}B_{20}$ amorphous alloy.[33] It is known that the presence of shoulder on the second diffuse peak of $S(q)$ is an evidence for a certain structural ordering in the amorphous phase.[33] The characteristic shoulder can be absent even for non-magnetic amorphous alloys like Pt-Ni-P,[34] Pt-P,[35] and La-Al-Ni.[36] Hence, the partial replacement of Ta with Y may increase the extent of the disorder in the $Co_{40}Fe_{22}Ta_{8-x}Y_xB_{30}$ glassy ribbons.

Besides the shape, addition of Y can affect the position of the diffraction maxima. Figure 5 shows the variation in positions of the first diffuse maxima (q_1) and the second one (q_2) of $S(q)$ as a function of Y content. Those positions were determined by fitting the top of the $S(q)$ peaks to the pseudo-Voigt function. It is observed that q_1 decreases continuously by introduction of Y, however, q_2 indicates a reverse behavior and it increases upon Y addition. As mentioned above, addition of Y affects the local ordering of the amorphous phase. It is known that the diffuse maxima of $S(q)$ with large q values determine the SRO constructed by solute-centered quasi-equivalent clusters.[37–39] On the other hands, the low-q part of $S(q)$ characterizes the packing and connection of the quasi-equivalent clusters or the medium-range order (MRO).[37–39] As inferred from Fig. 4, the observed changes in position and shape of the diffuse maxima particularly for the first and second peaks, can manifest that changes occurred in the MRO.

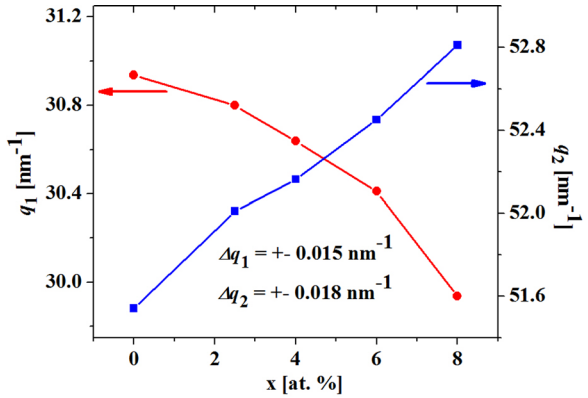

FIG. 5. Variations in positions of the first diffuse maxima (q_1) and the second one (q_2) of the structure factors $S(q)$ as a function of Y content.

The structural evolution of the $Co_{40}Fe_{22}Ta_{8-x}Y_xB_{30}$ glassy ribbons can be further investigated in the real-space by calculating the reduced pair correlation functions $G(r)$ according to Eq. (1). Figure 6 plots the $G(r)$ of the $Co_{40}Fe_{22}Ta_{8-x}Y_xB_{30}$ glassy ribbons. It is obvious that the Y addition induces significant changes in shape and intensity of the $G(r)$ peaks in the short-range and medium-range atomic correlations. As the figure shows, the Y free alloy indicates pronounced oscillations up to $r \approx 1.6\,nm$, demonstrating a high degree of MRO. However, addition of Y decreases noticeably the intensity of $G(r)$ peaks in the medium-range scale, which results in a faster decay of oscillations and decreasing the corresponding correlation length (Fig. 7). In other words, the degree of the MRO decreases in the Y bearing glassy alloys, in a good agreement with the reciprocal-space results (Fig. 4). Furthermore, the splitting of the second $G(r)$ peak can be observed in each composition. It is obvious that the intensity of the right shoulder of the second $G(r)$ increases by introduction of Y. This effect implies that the atoms prefer to place at larger distances in the second near-neighbor shell, probably because of large atomic radii of Y compared to other elements.

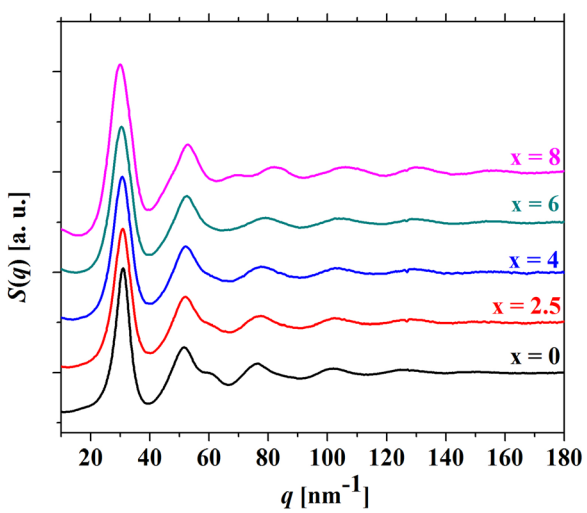

FIG. 4. The XRD total structure factors $S(q)$ of the $Co_{40}Fe_{22}Ta_{8-x}Y_xB_{30}$ (x = 0, 2.5, 4, 6, and 8) glassy ribbons.

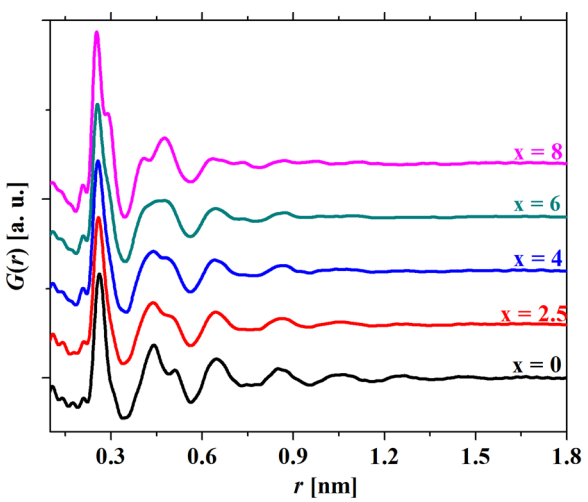

FIG. 6. The reduced pair correlation functions $G(r)$ of the $Co_{40}Fe_{22}Ta_{8-x}Y_xB_{30}$ (x = 0, 2.5, 4, 6, and 8) glassy ribbons.

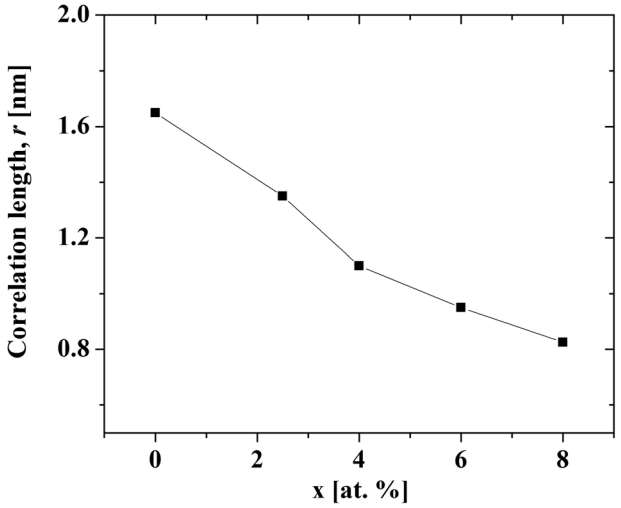

FIG. 7. Evolution of the correlation length for the $Co_{40}Fe_{22}Ta_{8-x}Y_xB_{30}$ (x = 0, 2.5, 4, 6, and 8) glassy ribbons with respect to Y fraction.

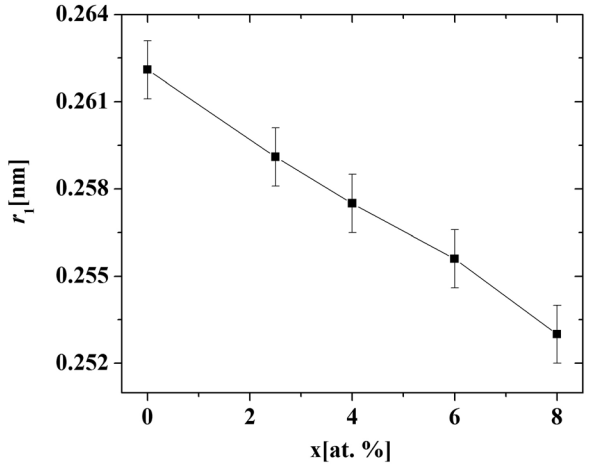

FIG. 9. Variations in position for the first peak of the pair correlation functions $G(r)$ of the $Co_{40}Fe_{22}Ta_{8-x}Y_xB_{30}$ (x = 0, 2.5, 4, 6, and 8) glassy ribbons as a function of Y fraction.

Figure 8 depicts the evolution of $G(r)$ in the range of the first coordination shell of the $Co_{40}Fe_{22}Ta_{8-x}Y_xB_{30}$ glassy ribbons. In addition, the inter-atomic bond lengths, calculated from sum of the Goldschmidt's radii, are presented. All the plots indicate a pre-peak at $r \approx 0.21$ nm, due to formation of (Co,Fe)-B pairs in the glassy structure. It should be emphasized that the contributions of Fe and Co atoms are indistinguishable owing to their similar atomic radii. According to the type and concentration of the constituent elements, it can be inferred that the maximum of the first $G(r)$ peak in all compositions dominantly consists of (Co,Fe)-(Co,Fe) pairs. In the 5 component alloys containing both Y and Ta, there are 15 overlapping atomic pairs in the first coordination shell. It is worth to note that with only one total atomic pair density distribution function, it is not possible to distinguish all of partial atomic pair correlations. The overlapping of the atomic pairs results in a non-asymmetric first $G(r)$ peak and appearance of a strong right-hand shoulder, particularly for Ta free alloy, as can be seen in Fig. 8. Besides the significant

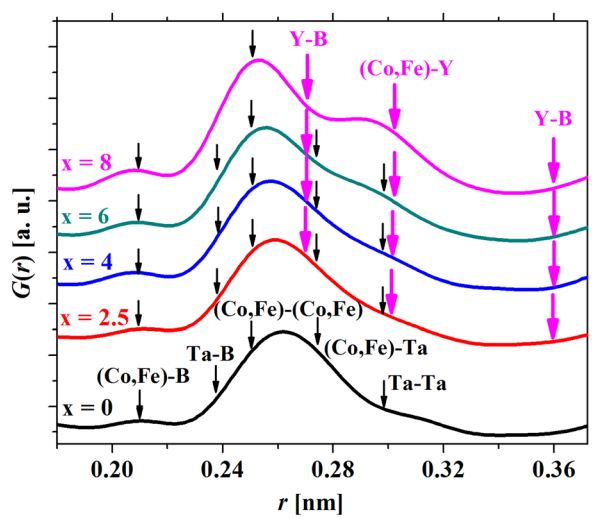

FIG. 8. The reduced pair correlation functions $G(r)$ of the $Co_{40}Fe_{22}Ta_{8-x}Y_xB_{30}$ (x = 0, 2.5, 4, 6, and 8) glassy ribbons depicted in the range of the first coordination shell.

changes in the shape of the main $G(r)$ peak, addition of Y changes the position of its maximum. According to Fig. 9, the position of the maximum of the first $G(r)$ peak decreases almost linearly with increasing the Y fraction. This may imply that the (Co,Fe)-(Co,Fe) pair separation decreases by Y addition and it approaches the theoretical (Co,Fe)-(Co,Fe) bond length (0.25 nm), obtained as a sum of atomic radii. It is worth to note that a similar contraction of the dominant inter-atomic distance happens for Fe-Fe atomic pairs in the $Fe_{70}Co_{10}B_{20}$ glasses upon partial replacement of the Fe atoms with some lanthanide elements.[33]

It is known that the building blocks or SRO in MGs can be identified as the Kasper-type (quasi-equivalent) solute-centered coordination polyhedra.[39] The type of such polyhedral is controlled by the effective atomic size ratio between the solute and solvent atoms, R^*.[39] With decreasing R^*, the preferred polyhedral type changes from the Frank–Kasper type (for $R^* > 1.2$) to the icosahedral type ($R^* < 0.902$), then to the bi-capped square Archimedean antiprism (BSAP) type ($R^* < 0.835$) and finally to the tri-capped trigonal prism (TTP) type ($R^* < 0.732$).[39] In the current alloying system, the R^* between B as the main solute atom and Co as the solvent atom is 0.69. Hence, it is anticipated that the chemical SRO in the $Co_{40}Fe_{22}Ta_{8-x}Y_xB_{30}$ glassy ribbons is probably made of B-centered TTP polyhedra. It has been shown that B-centered-TTP polyhedra with a Voronoi index of $\langle 0,3,6,0 \rangle$ is the dominant polyhedra in the SRO of the $Co_{43}Fe_{20}Ta_{5.5}B_{31.5}$ MG, which has a similar composition to the glassy alloys in this work.[40] The TTP polyhedra in metal-metalloid type MGs are the ideal blocks for constructing the network-like MRO.[40] Formation of the network-like structure can be correlated not only to the necessity of dense packing but also to the chemical interactions and the directionality of the covalent bonds in metal-metalloid pairs.[40] For the $Co_{43}Fe_{20}Ta_{5.5}B_{31.5}$ MG, it has been shown that the B-centered network-like MRO can be built through the connection of the TTP polyhedra via vertex-, edge-, face-, and intercross-shared atoms and all four kinds of component elements can serve as glue atoms.[40] A minor introduction of the glue elements with very large atomic radii like Y can distort

the TTP polyhedra and slightly change their arrangement. On the other hand, the excessive addition of Y could introduce large internal strains and hence break the network-like structure and consequently decrease the degree of such MRO (see Figs. 6 and 7). A continuous decrease of thermal stability upon addition of Y beyond 2.5 at. % (Table I) could be attributed to decrease in the extent of the network-like MRO, which has a different atomic configuration compared to the precipitating $(Co,Fe)_{21}(Ta,Y)_2B_6$ crystal.

C. Magnetic properties

Figure 10 shows the evolution of the saturation magnetization (normalized) as a function of temperature, measured at a constant heating rate of 10 K/min. As the figure shows, the magnetization drops for each sample and passes through an inflection point attributed to the Curie temperature T_c of the glassy phase and then it becomes spontaneously zero. According to Fig. 10, the inflection point moves to higher temperatures by increasing the Y fraction, which implies the enhancement of T_c. The T_c of the ribbons were determined accurately according to the approach proposed by Herzer,[41] through plotting the $(M_s)^{1/\beta}$ versus T ($\beta = 0.36$). T_c was measured as the temperature in which $(M_s)^{1/\beta}$ deviates from linearity. Table I lists the T_c of the $Co_{40}Fe_{22}Ta_{8-x}Y_xB_{30}$ ribbons. The changes in T_c are correlated with the exchange integral J_{ex}, which depends on the inter-atomic distances.[42] The increase of T_c upon addition of Y reveals that exchange interactions between the ferromagnetic elements become stronger probably due to the decrease in the (Co,Fe)–(Co,Fe) inter-atomic distance (see Fig. 9). Furthermore, the variations in T_c after introducing the Y atoms can be attributed to the changes in the coordination number of the ferromagnetic elements,[42] which cannot be determined with only one total atomic pair density distribution function.

Figure 11 depicts the *M-H* hysteresis loops of the $Co_{40}Fe_{22}Ta_{8-x}Y_xB_{30}$ ribbons. All the glassy ribbons exhibit a rectangular hysteresis curve, characteristic to soft magnetic materials. The rectangular tendency is a consequence of high magnetic permeability and low demagnetizing field, due to the small thickness of the ribbons compared to their other dimensions.[43] According to Fig. 11 and Table I, it is observed that the saturation magnetization M_s of the glassy ribbons increases with a similar trend as found for T_c with addition of Y. Since M_s also depends on the exchange interactions between the ferromagnetic elements, it is plausible that it follows the trend of T_c upon Y addition. Despite the inter-atomic distance, the significant changes in saturation magnetization and Curie temperature of these ribbons can originate from different electronic structure of Ta and Y atoms. The number of valence electrons in Ta and Y is 3 and 1, respectively. Hence, it is anticipated that the charge transferred to the d bands of Fe or Co atoms may decrease by introduction of Y atoms and consequently the ferromagnetic atoms have larger magnetic moments in compositions with larger Y content. The suppression of the magnetic moment of the Co atoms in the Co-based alloys after alloying with non-ferromagnetic transition metals has been described by Friedel's virtual-bound-state (VBS) model.[11,44] According to this model, the VBS for the transitions metals with strong perturbing potential (with a valence difference $\Delta Z > 2$) could move above the Fermi energy.[11] Consequently, the magnetic moment of Co atoms decreases due to the charge transfer from the VBS of the non-magnetic transition metals (like Ta and Y) into the d-band of Co based on the following equation:[11]

$$\frac{d\mu_{Co}}{dC} = -(10 + \Delta Z)\mu_B, \tag{2}$$

where C is the fraction of the non-ferromagnetic atom. It can be seen that the moment reduction is $-6\,\mu_B$ and $-4\,\mu_B$ for addition of Ta and Y, respectively. Hence, the larger magnetic moment of Co atoms can also contribute to the enhancement of the saturation magnetization and Curie temperature of these compositions upon alloying with Y. Furthermore, the $Co_{40}Fe_{22}Ta_{8-x}Y_xB_{30}$ glassy ribbons exhibit very small coercivity H_c (see Table I), proving their very good soft magnetic behavior. The small H_c of these ribbons proves the formation of homogeneous glassy structures with very small magnetocrystalline anisotropy. In addition, very low values of H_c could be also attributed to the small stress-induced anisotropy because of very small magnetostriction

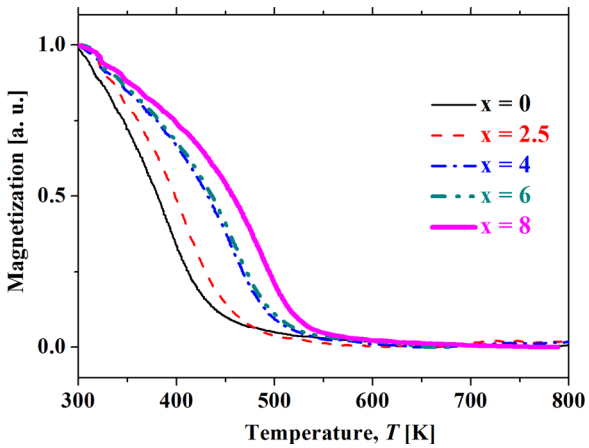

FIG. 10. The thermomagnetic plots of the $Co_{40}Fe_{22}Ta_{8-x}Y_xB_{30}$ (x = 0, 2.5, 4, 6, and 8) glassy ribbons obtained at a constant heating rate of 10 K/min.

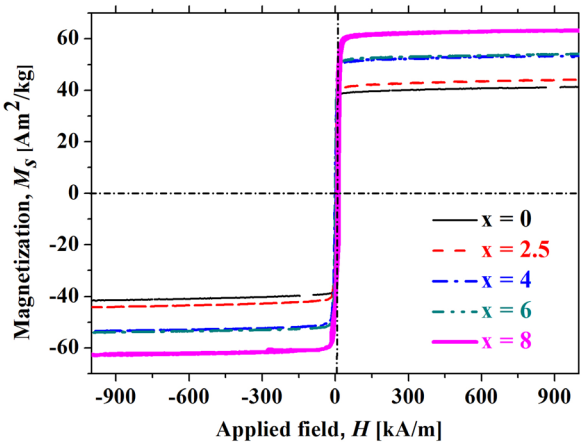

FIG. 11. The *M-H* hysteresis curves of the $Co_{40}Fe_{22}Ta_{8-x}Y_xB_{30}$ (x = 0, 2.5, 4, 6, and 8) glassy ribbons.

coefficient constant, which is in the order of $\lambda \approx 10^{-7}$ ppm for the Co-based glassy alloys.[11]

According to above results, alloy with $x = 2.5$ due to a large SLR and very good soft magnetic properties can be promising for the spark plasma sintering (SPS) or hot pressing processes, in order to produce the bulk glassy alloys with large size and complex shape by consolidation of the glassy powders in the temperature range of SLR, where the viscosity drops significantly.[1]

IV. CONCLUSIONS

The influence of Y addition on atomic structure, thermal stability, and magnetic properties of the $Co_{40}Fe_{22}Ta_{8-x}Y_xB_{30}$ MGs was investigated. The results indicated that the addition of 2.5 at. % Y noticeably improves the thermal stability through increasing the extension of the SLR, while the excessive alloying by Y deteriorates the thermal stability. Moreover, addition of Y decreases the degree of the network-like MRO probably due to the introduction of large internal strains. The decrease in thermal stability after extra addition of Y was attributed to the decrease in the extent of network-like MRO and fraction of the $(Co,Fe)_{21}(Ta,Y)_2B_6$ phase appeared upon primary crystallization. It was shown that the (Co,Fe)-(Co,Fe) pairs have shorter inter-atomic distance in the Y bearing alloys. This gives rise to stronger interactions between the ferromagnetic elements, which results in improving the saturation magnetization and Curie temperature.

ACKNOWLEDGMENTS

A. H. Taghvaei is thankful to IFW Dresden for the support of his stay and research in the frame of Ph.D. study at the Institute for Complex Materials. M. Stoica, I. Kaban, and U. Rütt are highly acknowledged for technical assistance. Parts of this research were carried out at the light source PETRA III at DESY (Hamburg, Germany), a member of the Helmholtz Association (HGF).

[1]C. Suryanarayana and A. Inoue, *Bulk Metallic Glasses* (CRC Press, Boca Raton, 2011).
[2]A. Inoue and A. Takeuchi, Acta Mater. **59**, 2243 (2011).
[3]Y. Q. Cheng and E. Ma, Prog. Mater. Sci. **56**, 379 (2011).
[4]W. H. Wang, Prog. Mater. Sci. **52**, 540 (2007).
[5]N. Zheng, R. T. Qu, S. Pauly, M. Calin, T. Gemming, Z. F. Zhang, and J. Eckert, Appl. Phys. Lett. **100**, 141901 (2012).
[6]Q. He, Y.-Q. Cheng, E. Ma, and J. Xu, Acta Mater. **59**, 202 (2011).
[7]C. C. Yuan and X. K. Xi, J. Appl. Phys. **109**, 033515 (2011).
[8]A. Inoue, B. L. Shen, H. Koshiba, H. Kato, and A. R. Yavari, Acta Mater. **52**, 1631 (2004).
[9]J. Swierczek, H. Lampa, Z. Nitkiewicz, and Z. Balaga, Mater. Sci. Eng., A **356**, 108 (2003).
[10]A. Inoue, B. L. Shen, and C. T. Chang, Intermetallics **14**, 936 (2006).
[11]M. E. McHenry, M. A. Willard, and D. E. Laughlin, Prog. Mater. Sci. **44**, 291 (1999).
[12]A. Inoue, T. Itoi, H. Koshiba, and A. Makino, IEEE. Trans. Magn. **35**, 3355 (1999).
[13]T. Itoi, T. Takamizawa, Y. Kawamura, and A. Inoue, Scr. Mater. **45**, 1131 (2001).
[14]A. Inoue, B. L. Shen, H. Koshiba, H. Kato, and A. R. Yavari, Nature Mater. **2**, 661 (2003).
[15]A. H. Taghvaei, M. Stoica, M. Samadi Khoshkhoo, I. Kaban, J. Bednarčik, P. Jóvári, K. Janghorban, and J. Eckert, Mater. Lett. **93**, 322 (2013).
[16]A. H. Taghvaei, M. Stoica, K. G. Prashanth, and J. Eckert, Acta Mater. **61**, 6609 (2013).
[17]*Metals Databook* (The Japan Institute of Metals, Maruzen, Tokyo, 2004), p. 8.
[18]A. Takeuchi and A. Inoue, Mater. Trans. JIM **46**, 2817 (2005).
[19]A. P. Hammersley, S. O. Svensson, M. Hanfland, A. N. Fitch, and D. Hausermann, High Pressure Res. **14**, 235 (1996).
[20]X. Qiu, J. W. Thompson, and S. J. L. Billinge, J. Appl. Crystallogr. **37**, 678 (2004).
[21]T. E. Faber and J. M. Zimman, Philos. Mag. **11**, 153 (1965).
[22]A. H. Taghvaei, M. Stoica, K. Song, K. Janghorban, and J. Eckert, J. Alloys Compd. **605**, 199 (2014).
[23]P. Villars and L. D. Calvert, *Pearson's Handbook of Crystallographic Data for Intermetallic Phases* (ASM International, Materials Park, Ohio, 1991), Vol. 2.
[24]J. Long, P. R. Ohodnicki, D. E. Laughlin, M. E. McHenry, T. Ohkubo, and K. Hono, J. Appl. Phys. **101**, 09N114 (2007).
[25]M. Widom and M. Mihalkovic, J. Mater. Res. **20**, 237 (2005).
[26]M. Imafuku, S. Sato, H. Koshiba, E. Matsubara, and A. Inoue, Mater. Trans. JIM **41**, 1526 (2002).
[27]M. Imafuku, S. Sato, H. Koshiba, E. Matsubara, and A. Inoue, Scr. Mater. **44**, 2369 (2001).
[28]E. Matsubara, S. Sato, M. Imafuku, T. Nakamura, H. Koshiba, A. Inoue, and Y. Waseda, Mater. Sci. Eng., A **312**, 136 (2001).
[29]S. J. Poon, G. J. Shiflet, F. Q. Guo, and V. Ponnambalam, J. Non-Cryst. Solids **317**, 1 (2003).
[30]I. Kaban, P. Jóvári, M. Stoica, J. Eckert, W. Hoyer, and B. Beuneu, Phys. Rev. B **79**, 212201 (2009).
[31]A. Seifoddini, M. Stoica, M. Nili-Ahmadabadi, S. Heshmati-Manesh, U. Kuhn, and J. Eckert, Mater. Sci. Eng., A **560**, 575 (2013).
[32]X. J. Gu, S. J. Poon, G. J. Shiflet, and M. Widom, Appl. Phys. Lett. **92**, 161910 (2008).
[33]M. Imafuku, K. Yaoita, S. Sato, W. Zhang, A. Inoue, and Y. Waseda, Mater. Sci. Eng., A **304–306**, 660 (2001).
[34]A. Shinha and P. Duwez, J. Phys. Chem. Solids **32**, 267 (1971).
[35]H. S. Chen, Y. Waseda, and K. T. Aust, Phys. Status Solidi A **65**, 695 (1981).
[36]E. Matsubara, T. Tamura, Y. Waseda, T. Zhang, A. Inoue, and T. Masumoto, J. Non-Cryst. Solids **150**, 380 (1992).
[37]G. S. Cargill III, Solid State Phys. **30**, 227 (1975).
[38]Y. Suzuki, J. Haimovich, and T. Egami, Phys. Rev. B **35**, 2162 (1987).
[39]H. W. Sheng, W. K. Luo, F. M. Alamgi, J. M. Bai, and E. Ma, Nature **439**, 419 (2006).
[40]X. Hui, D. Y. Lin, X. H. Chen, W. Y. Wang, Y. Wang, S. L. Shang, and Z. K. Liu, Scr. Mater. **68**, 257 (2013).
[41]G. Herzer, IEEE. Trans. Magn. **26**, 1397 (1990).
[42]R. O'Handley, J. Appl. Phys. **62**, R15 (1987).
[43]J. A. Osborn, Phys. Rev. **67**, 351 (1945).
[44]J. Friedel, Nuovo Cimento, Suppl. **7**, 287 (1958).